Photogrammetric Record, xx(xxx): 000–000 (Month 20##)

3D RECONSTRUCTION OF INTERNAL WOOD DECAY USING PHOTOGRAMMETRY AND SONIC TOMOGRAPHY

JUNJIE ZHANG* (junjiez@student.unimelb.edu.au)

KOUROSH KHOSHELHAM (k.khoshelham@unimelb.edu.au)

The University of Melbourne, Melbourne, Australia

* *Corresponding author*

Abstract

Knowledge of deteriorations within tree trunks is critical for arborists to conduct individual tree health assessments. Sonic tree tomography, a non-destructive technique using sound waves, has been widely used to estimate the size and shape of internal decay based on sound wave velocity variations. However, it has commonly been applied to 2D horizontal or vertical cross sections and its accuracy is questionable due to the poor approximation of the shape of the cross section. This paper proposes an integration of close-range photogrammetry and sonic tomography to enable accurate reconstruction of the exterior and interior of the tree trunk in 3D. The internal wood quality is represented by the spatially interpolated sound wave velocities, using the time of flight of the sound waves and the coordinates of the acoustic sensors obtained from the photogrammetric model.

Experimental results show that the proposed approach provides a realistic 3D visualisation of the size, shape and location of the internal deteriorations.

KEYWORDS: tree health, sonic tomography, photogrammetry, interpolation, sensor fusion.

INTRODUCTION

WOOD DETERIORATION WITHIN TREE TRUNKS affects the health of the trees and can pose a threat to the safety of pedestrians in urban areas, as they may topple over without warning. Such internal decay, caused by issues such as anaerobic bacteria, can decrease the mechanical (structural) properties of wood, yet it is often not visually apparent on the exterior of trees (Ross et al., 1992). Therefore, a method for detecting decay or cavities within tree trunks without permanently damaging them has been desired by arborists and forest managers (Wang et al., 2004).

Different techniques borrowed from medical science, including X-ray, neutron radiography, computer tomography and magnetic resonance, have been applied to tree health assessment in order to identify the deteriorations within trees (Wang et al., 2004). However, these methods are not ideal for arboriculture as they require expensive specialised equipment. Other techniques including ultrasonic tomography (Brancheriau et al., 2008), electrical resistivity (Al Hagrey, 2006), thermal imaging (Catena and Catena, 2008) and ground penetrating radar (Giannakis et al., 2019) have also been shown to have limitations in terms of reliability as well as time- and cost-efficiency. On the other hand, stress wave techniques have been shown to be effective in wood quality assessment (Ross and Pellerin, 1994) and have become popular in the industry for its cost efficiency and robustness (Göcke et al., 2007). Sonic or acoustic measurements, involving the emission of a sound wave from one sensor to another through the material of interest, can quantify the density or quality of the medium by measuring the velocity of the sound wave. This technique was introduced for tree health assessment in the 1990s (Ross et al., 1992) and extended to a tomographic visualisation by Rinn (2014), which was then frequently referred to as non-destructive stress wave imaging or sonic tree tomography.

Sonic tree tomography is based on the measurement of the time-of-flight (ToF) of the sound wave travelling through the tree trunk from one acoustic sensor to another (Rinn, 2014). When the sound wave travels through damaged wood, which has a lower density, its velocity will be decreased, hence increasing the measured ToF. Provided that the direct distances between the sensors are known or estimated, the approximate velocities of the sound waves can be computed. With redundant sonic measurements, a tomography of a cross section visualising the wood quality can be produced as shown in Fig. 1.

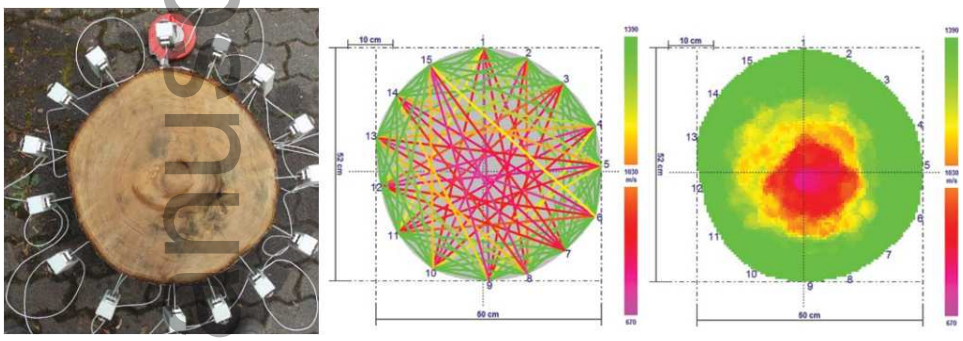

(a) (b) (c)

FIG. 1. Sonic tree tomography procedure: (a) typical setup of acoustic sensors; (b) measured velocities; (c) interpolated velocities showing decay at the centre (Rinn, 2015).

Conventional sonic tree tomography has two main limitations: (i) the analysis is limited to a 2D cross section, and (ii) the distances between sonic sensors cannot be directly measured. The common practice is to assume that the tree trunk is a cylinder and so the cross section is a perfect circle. The positions of the sonic sensors and the distances between them are then estimated using the circumference of the trunk (Feng et al., 2014). This introduces error to the analysis and makes the computed velocity of the sound waves inaccurate. Hence, the advantages of sonic tomography in terms of cost efficiency and data acquisition speed are compromised by the low accuracy of the computed sound wave velocity and the limitation of wood quality analysis to two dimensions (Nicolotti, 2003).

Automated photogrammetric workflows based on structure from motion (SfM) and dense matching enable rapid generation of 3D models of tree trunks to centimetre level precision (Furukawa and Ponce, 2010; Mokroš et al., 2018). This facilitates precise

localisation of the acoustic sensors for precise distance measurements. Using the 3D coordinates of the sonic sensors on the tree trunk, sound wave velocity can be precisely measured to generate a visualisation of wood quality in 3D.

This paper proposes a workflow based on the integration of sonic tree tomography and close-range photogrammetry for tree health assessment. The proposed workflow involves photogrammetric reconstruction of the exterior of the tree trunk, sound velocity measurement, and interpolation by ordinary kriging to create a 3D volumetric visualisation of the internal deteriorations of the tree.

AIMS AND OBJECTIVES

This paper aims to provide a method to improve the traditional sonic tree tomography, which is widely used to analyse tree health, by reconstructing the trunk and visualising the internal wood decay of a standing tree in 3D. The proposed method should achieve the following objectives:

(1) Produce distance measurements between sonic sensors to 1 cm precision (missing from sonic tree tomography), using close-range photogrammetry.
(2) Compute and spatially interpolate sound wave velocities to represent wood health.
(3) Visualise the realistic shape and size of the tree trunk, as well as the internal wood decay, in the form of 3D models.

BACKGROUND AND RELATED WORK

Ross et al. (1992) investigated bacterial infection within trees using non-destructive stress wave techniques. They quantified the wood quality within a felled log by measuring the time of flight (ToF) of the sound waves between two acoustic sensors mounted on the log. However, this test was limited to a 1D line segment and could not cover sufficient wood within a living tree.

Further development of sonic tree tomography included extending the acoustic measurements to multiple lines within a 2D cross section of the tree trunk (Rinn, 2014). The distance between two sensors was estimated using the circumference of the cross

section, assuming it to be a circle. Commercial products utilising this technology such as Arbotom developed by Rinntech (2019) allow adjustments to the shape of the cross section. However, the distances between the sensors are still determined based on an approximation.

Making acoustic measurements along straight lines results in gap regions in between the measurement lines as shown in Fig. 2. The velocity values within these gaps are typically determined by spatial interpolation. Among existing interpolation methods, kriging has been most commonly used in various sonic tree tomography products for estimating sound velocity values in gap regions from the measured values. Kriging is a statistical method suitable for *n*-dimensional interpolation where observations have directional correlation. For this reason, it has been preferred over other interpolation methods, such as inverse distance weighted (IDW), despite its higher computational cost (O'Sullivan and Unwin, 2010).

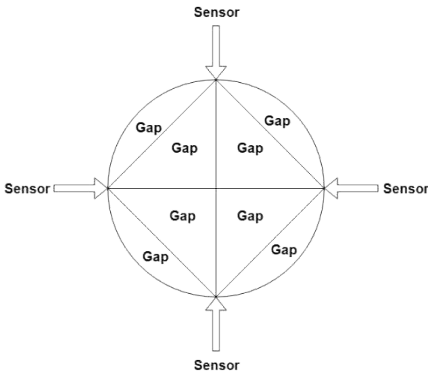

FIG. 2. Gaps between acoustic measurements in sonic tree tomography.

Kriging interpolation was used by Feng et al. (2014) to test sonic tree tomography, based on the assumption that the tree trunk was a cylindrical body and its cross section was an ideal circle. The circumference of the trunk was manually measured to estimate the distances between acoustic sensors and compute the sound wave velocities. The 2D cross section was then interpolated using ordinary kriging. The results showed that the interpolation produced acceptable estimates of internal decay in the tested trees. However, the estimated values were less reliable in deep cracks within the tree trunk, which was

recognised as a limitation of the technique. Another identified limitation was the deviation of the tested cross section of the tree from the expected shape, which was defined as a circle.

Du et al. (2018) attempted to improve the interpolation by employing top-*k* kriging (tkriging) and extending the interpolation to the third dimension. Tkriging attempts to identify the most relevant *k* observations and limits the interpolation to them. The results of Du et al. (2018) showed that kriging interpolation is applicable to sonic tree tomography in 3D.

Due to the anisotropic property of wood, sound waves do not necessarily propagate in straight lines (Du et al., 2015; Johnstone et al., 2010). The sound wave velocity can be impacted by the number of annual rings, angles between the acoustic sensors and the deviation of the cross section from the horizontal plane. It has been found that while reconstructing the wood quality of a tree trunk in 3D, the behaviour of the sound waves is significantly different on the longitudinal-radial plane (where 'longitudinal' is the vertical height direction) (Li et al., 2016). Therefore, care needs to be taken when computing the velocities of sound waves in 3D, as those crossing vertical heights are more complex than those on a horizontal cross section of the tree trunk.

The development of imaging methods including laser scanning and photogrammetry in recent decades has provided researchers with new ways of measuring trees. While laser scanning is (arguably) recognised as a more accurate technique, image-based modelling has been more commonly used for 3D reconstruction of trees due to its lower cost, the widespread availability of cameras and automated photogrammetric workflows (such as SfM). Bauwens et al. (2017) and Mokroš et al. (2018) tested automated photogrammetric workflows for modelling trees and measuring their dimensions. By using off-the-shelf cameras with a fixed focal length, 3D models of trees were produced with centimetre-level accuracies indicating that close-range photogrammetry is an appropriate technique to reconstruct the 3D shape of tree trunks and accurately measure their dimensions.

3D Reconstruction of Wood Decay

The proposed workflow involves 3D reconstruction of the interior and exterior of the tree trunk and consists of the following steps: data acquisition; photogrammetric reconstruction; computation of sonic velocities; and spatial interpolation. The following

sections describe the above steps of in detail.

Image Acquisition

To ensure that the 3D coordinates of the acoustic sensors can be measured accurately on the 3D model, the positions where the sensors will be mounted are marked with numbered targets prior to image acquisition. Fig. 3 shows a typical setup of the targets on the tree. To define the ground plane, four extra targets are placed around the tree on the ground. Several distances between the targets are measured to enable scaling the 3D model. Once the targets are placed, images are acquired with 60-80% overlap using a camera with fixed focal length which is self-calibrated within SfM. To ensure the success of the SfM algorithm, images are captured from different viewing angles and at different heights. Since accuracy is not a critical factor and the trees are usually free standing, there is no need to follow a strict image acquisition plan and the images can be taken simply from around the tree at a distance of 2 to 3 m.

FIG. 3. Targets placed to mark the position of sensors. Additional targets on the ground define the ground plane.

Time of Flight Measurement of Sound Waves

Time-of-flight measurements of sound waves are collected by using a stress-wave

imaging system such as Arbotom developed by Rinntech, Inc (Rinn, 2014). The sensors are placed at different horizontal levels at positions marked by the targets. Fig. 4 shows the sonic sensors mounted on the tree. Sound waves are generated by using a hammer to impact each sensor. Once a sensor is triggered, it starts the timer and emits stress waves to all the other sensors which, upon receiving the signals, stop the timer and report the time of flight to the software. The software stores the measured ToF in a matrix structure:

$$\mathbf{T} = \begin{bmatrix} 0 & t_{1,2} & \cdots & t_{1,n} \\ t_{2,1} & 0 & \cdots & t_{2,n} \\ \vdots & \vdots & \ddots & \vdots \\ t_{n,1} & t_{n,2} & \cdots & 0 \end{bmatrix} \quad (1)$$

where $t_{i,j}$ is the average ToF of the stress wave between acoustic sensors i and j. Note that there are two measured ToFs between each pair of sensors (in either direction), which are slightly different, due to the random errors in the measurements.

FIG. 4. Sonic sensors mounted on the tree.

Photogrammetric reconstruction of the exterior and extraction of sensor positions

For the 3D reconstruction existing SfM and dense matching algorithms implemented in software packages such as Agisoft PhotoScan/Metashape (Agisoft LLC, 2018) can be

used. The camera needs to be appropriately calibrated, which can be done in most photogrammetric software. Before computing the exterior orientation parameters, the target centres are measured and the measured distances are entered to scale the 3D model. Then, the exterior orientation parameters are computed, and a sparse point cloud is generated from the 3D coordinates of the tie points. Once the correctness of the exterior orientation process is verified, a dense point cloud is generated by applying a dense matching algorithm to the oriented images. Unnecessary parts of the point cloud are cropped out, and the cleaned point cloud is exported for further processing. The coordinates of the acoustic sensors can then be extracted from the reconstructed 3D model.

Computation of Sonic Velocities

Using the 3D coordinates of the sensors extracted in the previous step, the Euclidean distance between each pair of sensors, which is also the length of the propagated sound wave, is computed. The sound wave velocities $v_{i,j}$ are then computed as a symmetrical matrix, using the distance $d_{i,j}$ and mean of the two measured ToFs ($t_{i,j}$ and $t_{j,i}$) between each pair (i,j) of sensors:

$$\mathbf{V} = \begin{bmatrix} 0 & v_{1,2} & \cdots & v_{1,n} \\ v_{2,1} & 0 & \cdots & v_{2,n} \\ \vdots & \vdots & \ddots & \vdots \\ v_{n,1} & v_{n,2} & \cdots & 0 \end{bmatrix} = \begin{bmatrix} 0 & \frac{d_{1,2}}{(t_{1,2}+t_{2,1})/2} & \cdots & \frac{d_{1,n}}{(t_{1,n}+t_{n,1})/2} \\ \frac{d_{1,2}}{(t_{1,2}+t_{2,1})/2} & 0 & \cdots & \frac{d_{2,n}}{(t_{2,n}+t_{n,2})/2} \\ \vdots & \vdots & \ddots & \vdots \\ \frac{d_{n,1}}{(t_{n,1}+t_{1,n})/2} & \frac{d_{n,2}}{(t_{n,2}+t_{2,n})/2} & \cdots & 0 \end{bmatrix} \quad (2)$$

The above velocities are defined for straight lines connecting each pair of sensors. Considering that the sound velocity is not representative of the wood density along the whole line, only the velocity at the intersection of two lines is used for spatial interpolation. However, unlike the previous studies where lines would intersect on a 2D cross section (Feng et al., 2014), in the 3D space the lines connecting the sensors may not necessarily intersect, hence limiting the number of data points for interpolation. To overcome this limitation, the intersection points are defined as the mid-point of the shortest line segment

connecting each pair of nearly intersecting lines as shown in Fig. 5. Let the 3D line segment between two nearly intersecting lines be defined as:

$$\boldsymbol{p_2} = \boldsymbol{p_1} + t\vec{\boldsymbol{v}} \tag{3}$$

where $\vec{\boldsymbol{v}}$ is the direction vector of the line segment and t is a parameter that defines the position of point $\boldsymbol{p}_2$ with respect to point $\boldsymbol{p}_1$ on the line segment. Using the same expression for points $\boldsymbol{p}_1$ and $\boldsymbol{p}_2$ we can write:

$$\boldsymbol{p_b} + t_2\vec{\boldsymbol{v}}_2 = \boldsymbol{p_a} + t_1\vec{\boldsymbol{v}}_1 + t\vec{\boldsymbol{v}} \tag{4}$$

where $\boldsymbol{p}_a$ and $\boldsymbol{p}_b$ are 3D points representing the positions of sensors a and b respectively, and $\vec{\boldsymbol{v}}_1$ and $\vec{\boldsymbol{v}}_2$ are the direction vectors of the lines originating from these sensors. These direction vectors can be obtained from the coordinates of the sensor positions at the two ends of the corresponding lines, e.g., $\vec{\boldsymbol{v}}_1 = \boldsymbol{p_c} - \boldsymbol{p_a}$. The direction $\vec{\boldsymbol{v}}$ is perpendicular to $\vec{\boldsymbol{v}}_1$ and $\vec{\boldsymbol{v}}_2$ and is therefore obtained as the cross product of the two vectors: $\vec{\boldsymbol{v}} = \vec{\boldsymbol{v}}_1 \times \vec{\boldsymbol{v}}_2$. Thus, the three component equations in (4) can be solved for the three unknowns t_1, t_2, and t to obtain the points $\boldsymbol{p_1}$ and $\boldsymbol{p_2}$. Consequently, the coordinates of the mid-point of the shortest line segment between the two nearly intersecting lines is obtained as:

$$\boldsymbol{p} = \frac{\boldsymbol{p_1} + \boldsymbol{p_2}}{2} \tag{5}$$

Each mid-point is assigned the weighted average velocity of the corresponding nearly intersecting lines. Horizontal lines connecting sensors on the same height level receive a larger weight than those connecting sensors at different levels, because the velocities obtained for sensors at different height levels are considered less reliable due to the anisotropy of wood (Li et al., 2016). To ensure that the computed average velocity is reliable, the length of each shortest line segment is computed and those line segments whose lengths exceed an empirical threshold are eliminated from the process. In addition, mid-

points that fall too close to the sensors or outside the reconstructed 3D model of the trunk are deemed unreliable and excluded from the interpolation.

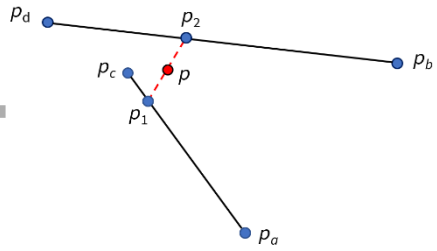

FIG. 5. Nearly intersecting lines and the corresponding control point p, which is defined as the mid-point of the shortest line segment p_1p_2 connecting each pair (p_ap_c and p_bp_d) of nearly intersecting lines.

Spatial Interpolation

The mid-points and the assigned velocities computed in the previous step are regarded as control points for the interpolation. A 3D grid consisting of regularly spaced points inside the 3D model of the trunk is constructed, and the velocities of the grid points are interpolated from the control points using the ordinary kriging interpolation method. Ordinary kriging begins by generating a semivariogram scatter plot representing the squared velocity differences between each pair of control points against the distances between the points (O'Sullivan and Unwin, 2010). The squared differences are the semivariances representing the spatial variation of the velocities. The semivariances are then grouped into 'lags' of certain distances and summarised by averaging the individual semivariances using the following equation:

$$2\hat{\gamma}(d) = \frac{1}{n\left(d \pm \frac{\Delta}{2}\right)} \sum_{d \pm \frac{\Delta}{2}} \left(v_i - v_j\right)^2 \tag{6}$$

where $\hat{\gamma}$ is the estimated semivariance, d is the selected distance between two points, Δ is the width of the defined lag, n is the number of points within the lag, and v_i and v_j are the known values at points i and j. The estimated semivariances represents the trend of the differences between the points against distance. The spatial variation revealed by the

semivariances is expressed by a semivariance function obtained by non-linear regression (O'Sullivan and Unwin, 2010). This semivariance function is then used to evaluate the semivariance for any given distance d. Finally, the interpolated value at a grid point s is obtained as:

$$v_s = \sum_{i=1}^{n} w_i v_i \tag{7}$$

where v_i is the velocity value of control point i, w_i is the weight of that control point, and n is the number of control points. The weights of the control points w_i are obtained by solving the following system of equations:

$$\begin{bmatrix} \gamma(d_{11}) & \gamma(d_{12}) & \cdots & \gamma(d_{1n}) & 1 \\ \vdots & \vdots & \ddots & \vdots & \vdots \\ \gamma(d_{n1}) & \gamma(d_{n1}) & \cdots & \gamma(d_{nn}) & 1 \\ 1 & 1 & \cdots & 1 & 0 \end{bmatrix} \times \begin{bmatrix} w_1 \\ \vdots \\ w_n \\ \lambda \end{bmatrix} = \begin{bmatrix} \gamma(d_{1p}) \\ \vdots \\ \gamma(d_{np}) \\ 1 \end{bmatrix} \tag{8}$$

where $\gamma(d_{ij})$ is the semivariance for distance d_{ij} obtained from equation (6), p is the point being interpolated, and λ is the Lagrangian multiplier. In equation (8) the last row of the coefficient matrix enforces the constraint that the sum of the weights of all control points must be 1.

Using the above procedure, the velocity at every grid point can be interpolated from the measured velocities of the control points. The interpolated velocities represent the health of the wood. The grid points are exported as a point cloud, representing the interior model of the tree trunk, and can be visualised in standard software such as CloudCompare (CloudCompare, 2019), to analyse the wood health at any horizontal or vertical cross section within the tree model.

While it is assumed that the interpolated velocities are approximately constant for healthy wood, some tree species exhibit internal variations in wood density resulting in variations in sound wave velocities (Göcke et al., 2007). However, these variations are significantly smaller than those caused by wood decay; therefore, changes in sound velocity provide a reliable indicator for wood decay.

EXPERIMENTAL SETUP

An experiment was conducted in Citizens Park, Richmond, Victoria, Australia to evaluate the proposed framework for 3D reconstruction of internal wood decay. A grown English elm (*Ulmus procera*) tree was selected for the experiment. An image of the tree can be seen in Fig. 3.

A Nikon D3100 camera with the AF-S DX NIKKOR 18-55 mm lens at a fixed focal length of 18 mm was used to capture the images of 4608 × 3072 pixels for the generation of the exterior model. To scale the model, distances between selected targets were obtained using a tape measure. An Arbotom system (Rinn, 2014) was used to collect the acoustic measurements. A total of 24 acoustic sensors were mounted on the positions marked by the targets at three height levels (90 cm, 120 cm and 150 cm above ground level) as shown in Fig. 4. The sensors were connected using cables, with the first and the last sensor connected to the battery pack, which transmitted the readings wirelessly to a computer with the Arbotom software.

The camera was calibrated using multiple images of a calibration pattern captured at different angles and the calibration parameters were computed in Agisoft PhotoScan (Agisoft LLC, 2018). The calibration parameters are listed in Table I. The pixel size of the camera sensor was identified as 0.005 mm. The images were captured at distances of 2 to 3 m from the tree, this resulted in a spatial resolution (sample distance) of 0.5 mm to 0.8 mm on the tree trunk. The same software was used to perform the image orientation and reconstruct a dense 3D model of the tree trunk. Using the 3D coordinates of the acoustic sensors extracted from the reconstructed model, distances between the sensors were computed and the ToF measurements were converted to sound wave velocity measurements.

TABLE I. Camera calibration parameters.

Focal length (mm)	*Principal point offset (pixels)*		*Radial distortion*			*Decentring distortion*	
f	c_x	c_y	k_1	k_2	k_3	p_1	p_2
18.33	3.92	-5.43	-9.94e-02	2.96e-02	-1.31e-03	-5.80e-05	2.13e-04

To generate the control points for interpolation, mid-points of near intersecting lines were computed. A threshold of 0.01 m was applied to exclude the mid-points of line segments that were not sufficiently small. For the weighted averaging of the velocity values a weight of 1.0 was used for horizontal lines between sensors at the same height level, and 0.75 for non-horizontal lines connecting sensors at different height levels. The data and procedure used in this experiment have been made publicly accessible (see https://github.com/zjjdes/treeReconstruction).

RESULTS AND DISCUSSION

Fig. 6(a) shows the reconstructed 3D model of the tree trunk, which was used to extract the coordinates of the acoustic sensors. An overall RMS error of 0.001 m was achieved for the image orientation task in Agisoft PhotoScan, indicating that a precision of better than 1 cm for the distance measurements between the acoustic sensors can be achieved. In total 276 ToF measurements were collected using Arbotom. Fig. 6(b) shows the velocity measurements overlaid on the 3D model. A total of 216 valid control points within the tree trunk were generated as a result using the parameters described above, of which 50 points were randomly selected as check points and the rest were used in the ordinary kriging process. Fig. 6(c) shows the computed control points overlaid on the 3D model.

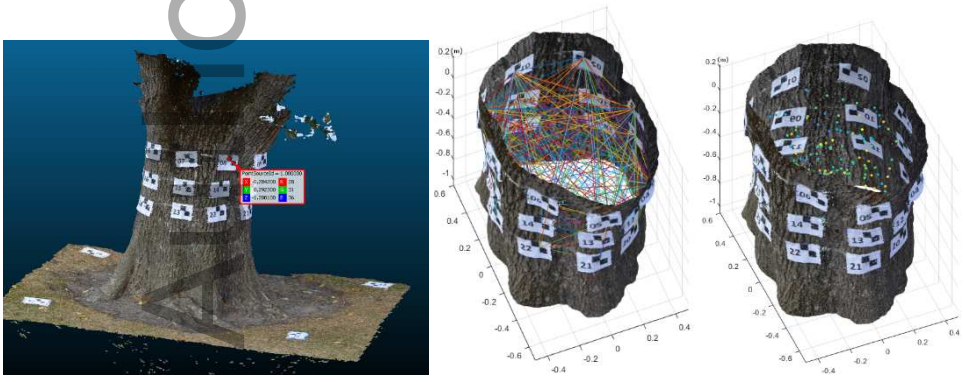

(a) (b) (c)

FIG. 6. 3D reconstruction and control point generation results: (a) extraction of sensor coordinates in CloudCompare; (b) sound velocity measurements overlaid on the 3D model; (c) valid control points overlaid on the 3D model.

Fig. 7 shows the semivariogram scatter plot generated from the control points, distance groups, and the non-linear regression performed using the Curve Fitting Toolbox in MATLAB (MathWorks, 2019). It can be seen that the semivariances are quite scattered, due to the fact that sound wave velocities change rapidly over short distances. Ordinary kriging interpolation was then performed using the control points and the semivariance function. Occasional negative weights, which are unavoidable in ordinary kriging (Deutsch, 1996), were removed and the remaining ones were standardised to sum to 1. The interpolated velocities representing the interior model are shown together with the exterior model in Fig. 8. The colours represent the interpolated sound wave velocities where higher values indicate better wood health.

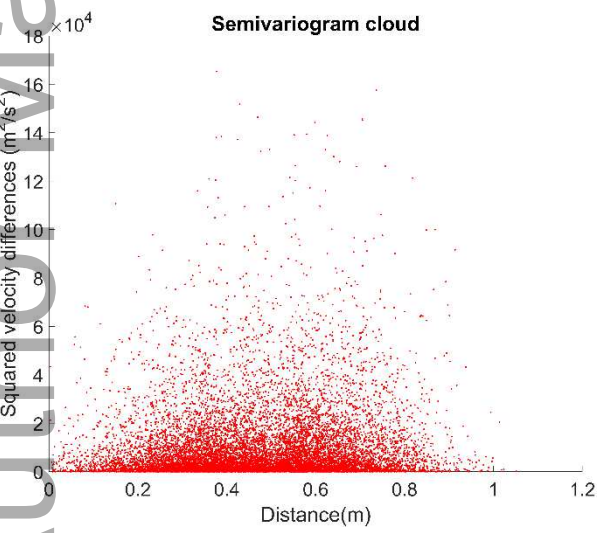

(a)

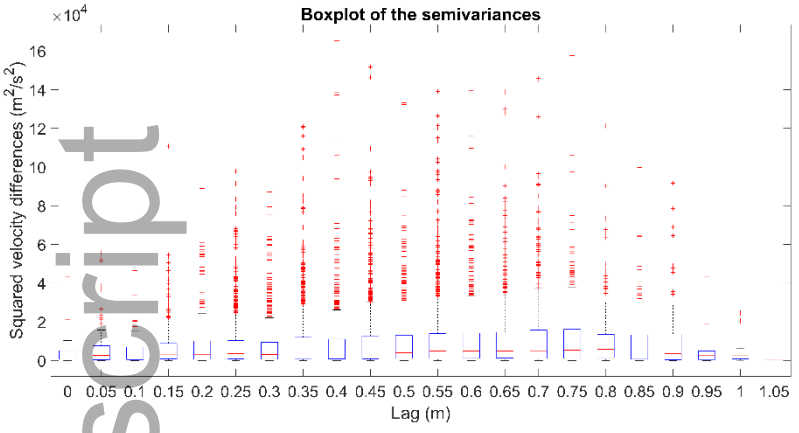

(b)

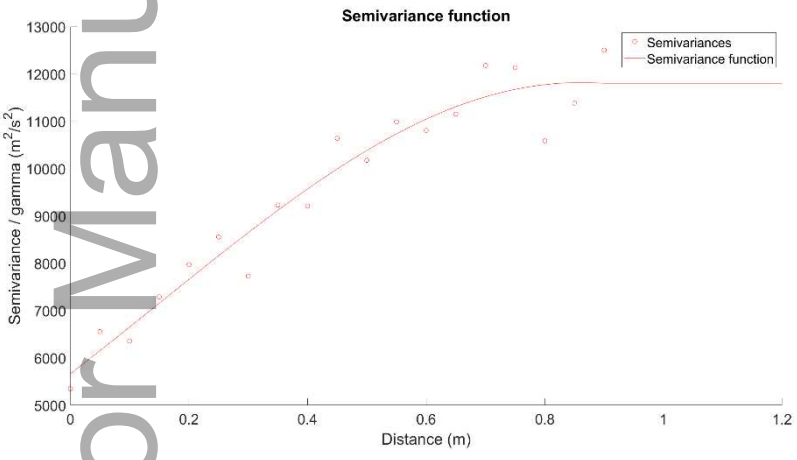

(c)

FIG. 7. Semivariance estimation: (a) semivariogram scatter plot; (b) semivariance box plot; (c) regression.

According to Fig. 7, in this experiment the semivariance function has a nugget of 5663.4m^2/s^2, a sill (maximum semivariance) of 11802.4m^2/s^2 and a range (distance when the semivariances reach the maximum) of 0.9 m (O'Sullivan and Unwin, 2010). In practice, this semivariance function produced negative weights during the interpolation. This was unacceptable as the weights must all be positive and their sum must be 1. However, Deutsch (1996) suggested that ordinary kriging does not guarantee positive weights and negative weights can arise when data close to the location being estimated screen outlying data.

Deutsch also proposed a method to adjust the weights by evaluating the covariances.

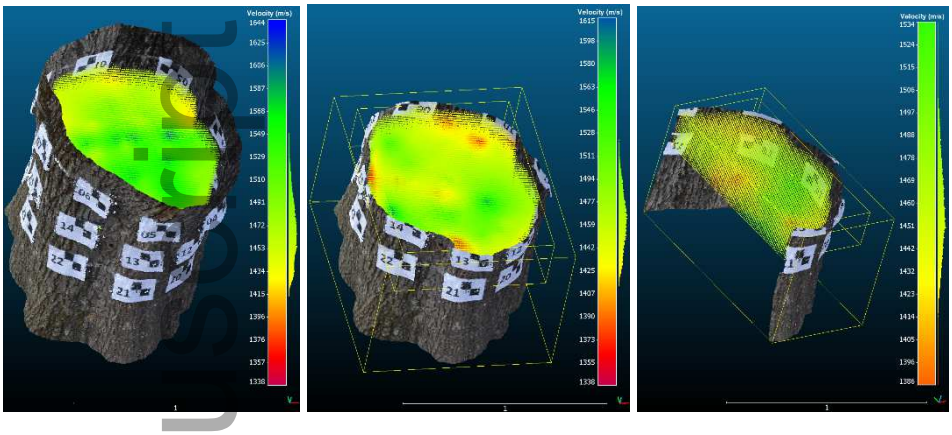

(a) (b) (c)

FIG. 8. Interpolated velocities overlaid on the 3D model: (a) the trunk model and the point cloud of interpolated velocities; (b) the models sliced horizontally; (c) the models sliced both horizontally and vertically. Lower velocities in red; higher velocities in blue.

In order to check the quality of the ordinary kriging interpolation, 50 random control points were excluded from the semivariance summarisation as check points. The same interpolation process was applied to these points so that they had both observed and interpolated velocities for comparison. Table II and Fig. 9 show the result of the comparison. Although there is a dramatic difference between the minimum (0.5 m/s) and the maximum velocity difference (201.3 m/s), the figure shows that the interpolated values are mostly in agreement with the observed values for the 50 check points. The root mean square error (RMSE) of these values is computed as 51.8 m/s. The sound wave velocities range from 1399.8 m/s to 1556.4 m/s and the mean interpolation error is around 2.5% of the maximum sound velocity, which can be considered acceptable.

TABLE II. Statistics of interpolation errors.

Min error (m/s)	*Max error (m/s)*	*Mean error (m/s)*	*Median error (m/s)*	*RMSE (m/s)*	*Mean error as percentage of max velocity (%)*

0.5	201.3	38.2	28.0	51.8	2.5%

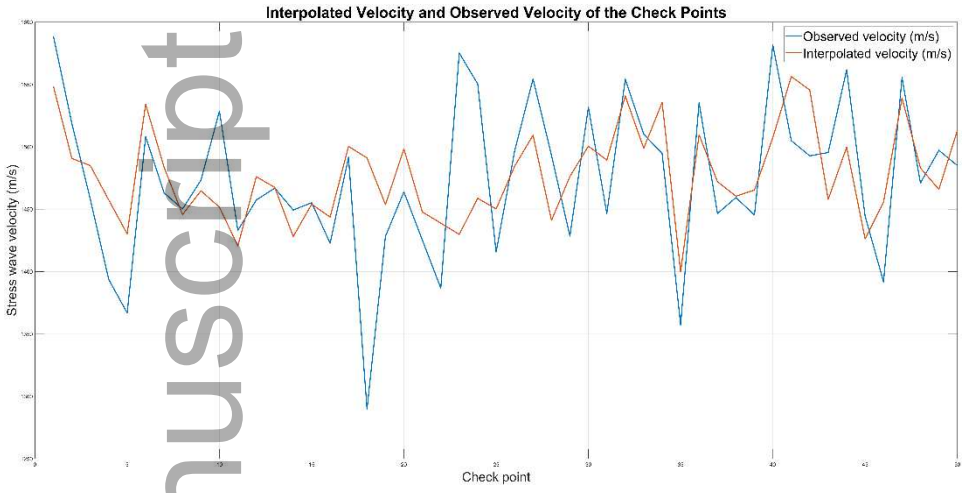

FIG. 9. Comparison between observed (blue) and interpolated (red) velocities.

Despite the presence of small errors in the interpolated velocity values, the impact of these errors is not critical, and by comparing the interpolated values of different parts of the tree trunk internal deteriorations can be identified when significant differences are present. In practice, the absolute velocity values are not important and internal deteriorations are identified based on variations in the velocity and the distributions of these variations (Göcke et al., 2007).

Fig. 10 shows cross sections of the generated exterior and interior models at approximately 90 cm, 120 cm and 150 cm from the ground, along with their counterparts retrieved from the proprietary software used in the Arbotom system, with warmer colours representing unhealthier wood. The main internal deteriorations detected by both methods are highlighted with red rings. It is apparent that the proposed 3D approach provides a significantly more accurate external shape of the tree trunk, as compared to the shape in the Arbotom software which was roughly estimated by the arborist. It can be seen on the cross section at 150 cm that both methods show nearly no deteriorations. On the cross sections at 90 cm and 120 cm respectively, both methods found alerting wood quality and the internal decay they identified have similar degrees, sizes and shapes. On the 120 cm cross

section, both the 3D model and Arbotom show less healthy wood in the centre, with the 3D model showing more individual deteriorations near the outer trunk, especially towards the top-right. Considering the central decay identified by Arbotom exhibits a small extension towards the same direction, this difference could be due to the two methods interpreting the same observation differently. Finally, at 90 cm above the ground, the two methods agree that the wood health is the worst among the three cross sections and the decay is around the centre. On all three cross sections, Arbotom results show concentrated deteriorations while the ones found in the 3D model are more dispersed. Despite these minor discrepancies, the 3D results generally agree with the 2D results, showing the most severe internal decay on the 90 cm cross section above ground, and medium quality of wood on the 120 cm cross section, with similar sizes, shapes and locations. Since Arbotom is a popular tool in the industry and has been used in numerous studies on non-destructive testing (Li et al., 2016; Yang and Luo, 2011), it can be concluded that the proposed approach achieves satisfactory results in modelling the exterior and the internal wood health of tree trunks.

The generation of the 3D model of wood decay took around 30 minutes on a standard PC (i7, 6700K, 16GB RAM), with kriging being the most computationally complex part of the process. In comparison, Arbotom generated the results within a few minutes. This indicates the lower computational efficiency of the proposed 3D approach, but also that there is room for improvement to optimise the proposed algorithm for better execution speed.

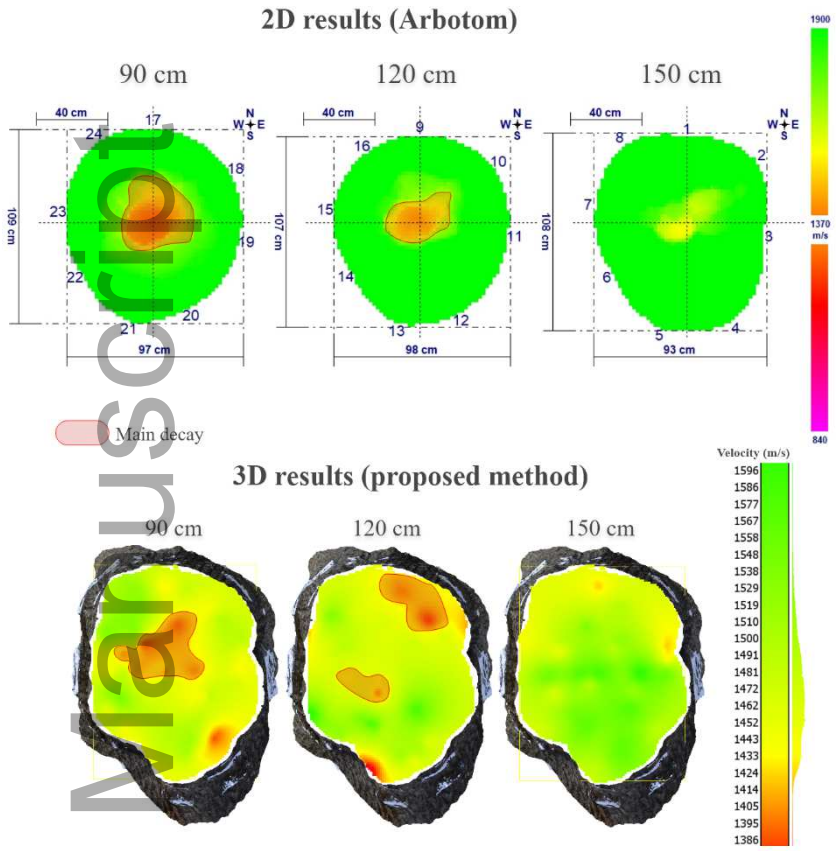

FIG. 10. The reconstructed 3D model of wood decay (bottom) compared with 2D results from a commercial software (Arbotom; top)) on three cross sections (90, 120 and 150 cm above ground level). Main decay depicted in orange and red.

CONCLUSIONS

This paper proposes an integration of sonic tomography and close-range photogrammetry for accurate 3D reconstruction of the exterior and internal decay of tree trunks. The photogrammetric reconstruction enables accurate measurement of the distances between the acoustic sensors, resulting in more accurate measurement of sound velocity and a more reliable assessment of wood quality. The proposed approach extends the traditional 2D visualisation to a 3D representation of the shape of the tree trunk and its internal deteriorations. It was experimentally shown that the size, shape and location of the

internal decay identified by the proposed approach mostly agree with those found by the traditional 2D approach, with the damaged wood visualised in more dispersed locations in the 3D approach. A limitation of the research was that the tree used in the experiment could not be sliced to expose the internal deteriorations for validation. Further research and experiments should have this as a priority in order to verify the feasibility of the proposed method. Future research should also focus on modifying the sound wave velocity computation and the interpolation process to accommodate the special properties of wood, such as its anisotropy, which can affect the behaviour of sound waves, as well as optimising the proposed algorithm to reduce the time required for processing.

ACKNOWLEDGEMENTS

This research was supported by The University of Melbourne through the Melbourne Research Scholarship awarded to the first author. The authors would also like to acknowledge the assistance towards the experiment from Mr David Galwey of Tree Dimensions, Melbourne, Australia.

REFERENCES

AGISOFT LLC, 2018. https://www.agisoft.com/pdf/photoscan-pro_1_4_en.pdf [Accessed 26th April 2019].

AL HAGREY, S. A., 2006. Electrical resistivity imaging of tree trunks. *Near Surface Geophysics*, 4(3): 179-187.

BAUWENS, S., FAYOLLE, A., GOURLET-FLEURY, S., NDJELE, L. M., MENGAL, C. and LEJEUNE, P., 2017. Terrestrial photogrammetry: a non-destructive method for modelling irregularly shaped tropical tree trunks. *Methods in Ecology and Evolution*, 8(4): 460-471.

BRANCHERIAU, L., LASAYGUES, P., DEBIEU, E. and LEFEBVRE, J. P., 2008. Ultrasonic tomography of green wood using a non-parametric imaging algorithm with reflected waves. *Annals of Forest Science*, 65(7): article 712. 7 pages.

CATENA, A. and CATENA, G., 2008. Overview of thermal imaging for tree assessment. *Arboricultural Journal*, 30(4): 259-270.

CLOUDCOMPARE, 2019. *CloudCompare Version 2.6.1 User Manual*. http://www.cloudcompare.org/doc/qCC/CloudCompare%20v2.6.1%20-%20User%20manual.pdf [Accessed 26th April 2019].

DEUTSCH, C. V., 1996. Correcting for negative weights in ordinary kriging. *Computers & Geosciences*, 22(7): 765-773.

DU, X., FENG, H., HU, M., FANG, Y. and CHEN, S., 2018. Three-dimensional stress wave imaging of wood internal defects using TKriging method. *Computers and Electronics in Agriculture*, 148: 63-71.

DU, X., LI, S., LI, G., FENG, H. and CHEN, S., 2015. Stress wave tomography of wood internal defects using ellipse-based spatial interpolation and velocity compensation. *BioResources*, 10(3): 3948-3962.

FENG, H., LI, G., FU, S. and WANG, X., 2014. Tomographic image reconstruction using an interpolation method for tree decay detection. *BioResources*, 9(2): 3248-3263.

FURUKAWA, Y. and PONCE, J., 2010. Accurate, dense, and robust multiview stereopsis. *IEEE Transactions on Pattern Analysis and Machine Intelligence*, 32(8): 1362-1376.

GIANNAKIS, I., TOSTI, F., LANTINI, L. and ALANI, A. M., 2019. Health monitoring of tree trunks using ground penetrating radar. *IEEE Transactions on Geoscience and Remote Sensing*, 57(10): 8317-8326.

GÖCKE, L., RUST, S., WEIHS, U., GÜNTHER, T. and RUCKER, C., 2007. Combining sonic and electrical impedance tomography for the nondestructive testing of trees. *15th International Symposium on Nondestructive Testing of Wood*, Duluth, Minnesota, USA. Pages 31-42.

JOHNSTONE, D., MOORE, G., TAUSZ, M. and NICOLAS, M., 2010. The measurement of wood decay in landscape trees. *Arboriculture & Urban Forestry*, 36(3): 121-127.

LI, G., WENG, X., DU, X., WANG, X. and FENG, H., 2016. Stress wave velocity patterns in the longitudinal–radial plane of trees for defect diagnosis. *Computers and Electronics in Agriculture*, 124: 23-28.

MATHWORKS, 2019. *MathWorks Curve Fitting Toolbox*. https://au.mathworks.com/products/curvefitting.html [Accessed 10th September 2019].

MOKROŠ, M., VÝBOŠŤOK, J., TOMAŠT'OK, J., GRZNÁROVÁ, A., VALENT, P., SLAVÍK, M. and MERGANIČ, J., 2018. High precision individual tree diameter and perimeter estimation from close-range photogrammetry. *Forests*, 9(11): article 696. 12 pages.

NICOLOTTI, G., SOCCO, L. V., MARTINIS, R., GODIO, A. and SAMBUELLI, L., 2003. Application and comparison of three tomographic techniques for detection of decay in trees. *Journal of Arboriculture*, 29(2): 66-78.

O'SULLIVAN, D. and UNWIN, D., 2010. Knowing the unknowable: the statistics of fileds. Chapter 10 in *Geographic Information Analysis*. 2nd edition. Wiley, Hoboken, New Jersey, USA. 432 pages: 287-312.

RINN, F., 2014. Central basics of sonic tree tomography. *Journal of the Society of Commercial Arborists (SCA-Today)*, 19(4): 8-10.

RINN, F., 2015. Central defects in sonic tree tomography. *Western Arborist*, 20: 38-41.

RINNTECH., 2019. *Arbotom* http://www.rinntech.de/content/view/7/35/lang,english/index.html [Accessed 20th April 2019].

ROSS, R. J. and PELLERIN, R. F., 1994. Nondestructive testing for assessing wood members in structures: a review. *General Technical Report FPL-GTR-70*. US Department of Agriculture, Forest Service, Forest Products Laboratory, Madison, Wisconsin, USA. 40 pages.

ROSS, R. J., WARD, J. C. and TENWOLDE, A., 1992. Identifying bacterially infected oak by stress wave nondestructive evaluation. *General Technical Report FPL-GTR-512*. US Department of Agriculture, Forest Service, Forest Products Laboratory, Madison, Wisconsin, USA. 6 pages.

WANG, X., DIVOS, F., PILON, C., BRASHAW, B. K., ROSS, R. J. and PELLERIN, R. F., 2004. Assessment of decay in standing timber using stress wave timing nondestructive evaluation tools: A guide for use and interpretation. *General Technical Report FPL-GTR-147*. US Department of Agriculture, Forest Service, Forest Products Laboratory, Madison, Wisconsin, USA. 12 pages.

YANG, X. and LUO, J., 2011. Study on stress wave non-destructive testing of compression resistance characteristics of logs. *IEEE International Conference on Transportation, Mechanical, and Electrical Engineering (TMEE)*, Changchun, China. Pages 874-878.

Résumé

La connaissance des détériorations à l'intérieur des troncs d'arbres est essentielle pour que les arboriculteurs puissent évaluer la santé de chaque arbre. La tomographie ultrasonore, une technique non destructive utilisant des ondes sonores, est largement utilisée pour estimer la taille et la forme de la dégradation interne à partir des variations de vitesse des ondes sonores. Cependant, elle est le plus souvent appliquée aux coupes 2D horizontales ou verticales, et sa précision est discutable en raison de la mauvaise approximation de la forme en coupe. Cet article propose une intégration de la photogrammétrie rapprochée et de la tomographie ultrasonore en vue d'une reconstruction précise en 3D de l'extérieur et de l'intérieur du tronc d'arbre. La qualité interne du bois est représentée par les vitesses des ondes sonores interpolées spatialement, en utilisant le temps de vol des ondes sonores ainsi que les coordonnées des capteurs acoustiques issues du modèle photogrammétrique. Les résultats expérimentaux montrent que l'approche proposée fournit une visualisation 3D réaliste de la taille, de la forme et de la localisation des détériorations internes.

Zusammenfassung

Kenntnisse über Schädigungen in Baumstämmen sind für Baumpfleger sehr wichtig, um die Gesundheit einzelner Bäume beurteilen zu können. Schall-Tomography für Bäume ist eine nicht zerstörende Technik, die benützt wird, um die Größe und Form von Fäulnisprozessen im Bauminneren auf Basis von Variationen in der Schallgeschwindigkeit, zu ermitteln. Allerdings wird diese Technik auf 2D horizontale oder vertikale Querschnitte angewandt und ihre Genauigkeit ist angesichts einer schwachen Annäherung der Form der Querschnitte in Zweifel zu ziehen. Deshalb wird hier eine Integration von Nahbereichsphotogrammetrie und Schall-Tomography vorgeschlagen, um eine genaue Rekonstruktion des Baumes außen und innen in 3D zu ermöglichen. Die interne Holzqualität wird durch die räumlich interpolierten Schallgeschwindigkeitsvariationen repräsentiert. Hierzu werden die Laufzeit der Schallwellen und die Koordinaten des Akustiksensors aus dem photogrammetrischen Modell verwendet. Die experimentellen Ergebnisse zeigen, dass der vorgeschlagene Ansatz eine realistische 3D-Visualisierung von Größe. Form und Position der internen Schädigungen ermöglicht.

Resumen

La medición y conocimiento del estado interno de los troncos de los árboles y su deterioro es fundamental para evaluar la salud de estos individualmente. La tomografía sónica de árboles, una técnica no destructiva que utiliza ondas sonoras, se ha utilizado ampliamente para estimar el tamaño y la forma del deterioro interno en función de las variaciones de velocidad de las ondas sonoras. Sin embargo, se ha aplicado comúnmente a secciones transversales horizontales o verticales 2D cuya precisión es cuestionable debido a la mala aproximación de la forma de la sección transversal. Este artículo propone una integración de la fotogrametría de objeto cercano y la tomografía sónica para alcanzar la reconstrucción 3D precisa del exterior e interior del tronco del árbol. La calidad interna de la madera se representa por la velocidad de las ondas sonoras, la cual se interpola espacialmente utilizando el tiempo de vuelo de las ondas sonoras y las coordenadas de los sensores acústicos obtenidos del modelo fotogramétrico. Los resultados experimentales muestran que el enfoque propuesto proporciona una visualización realista en 3D del tamaño, la forma y la ubicación de los deterioros internos en los troncos.

摘要

对树干内部缺陷的认知对于树木研究者进行单棵树木健康检查有关键性作用。应力波断层成像，一种利用声波的无损检测技术，基于声波速度的变化被广泛用于估测树干内部缺陷的尺寸和形状。然而该技术通常被用于 2D 水平或垂直截面，其准确度也因为对于截面形状的粗略估计而存疑。本文提出一种结合近景摄影测量和应力波断层成像的方法以实现对树干外部及内部的 3D 重建。将声波传播时间和从摄影测量模型上获取的应力波传感器坐标用于计算，内部木材质量以空间

插值计算的声波速度形式呈现。实验结果表明本文提出的方法可以实现对树干内部缺陷的尺寸、形状和位置的拟真 3D 重建。

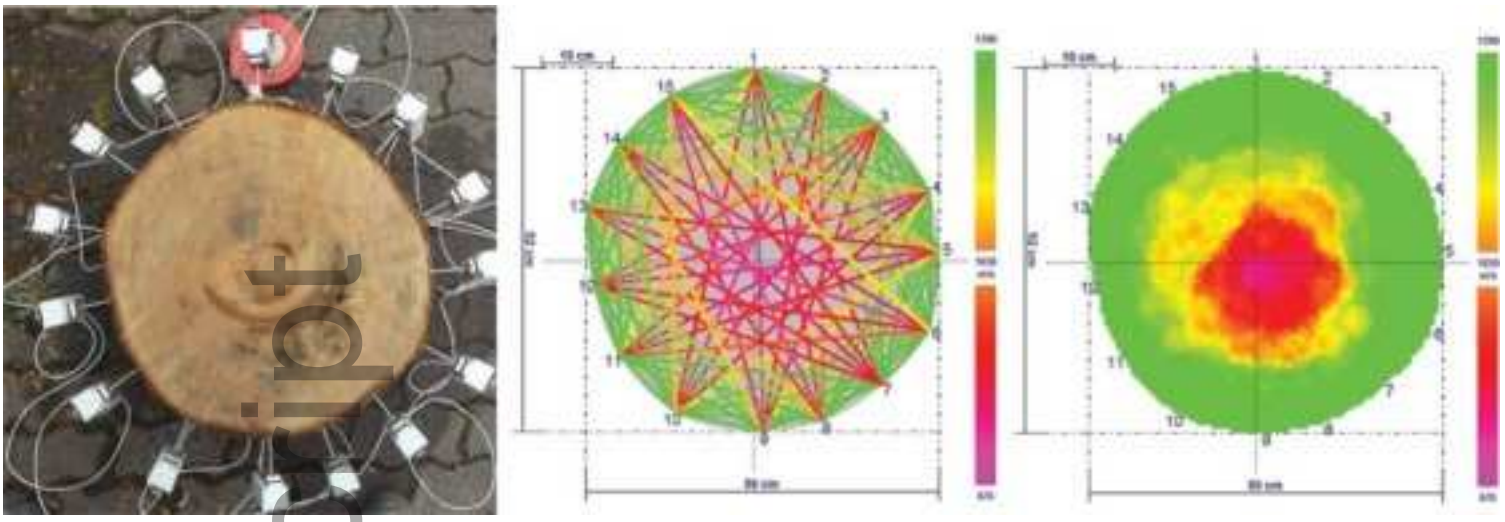

phor_12328_f1.png

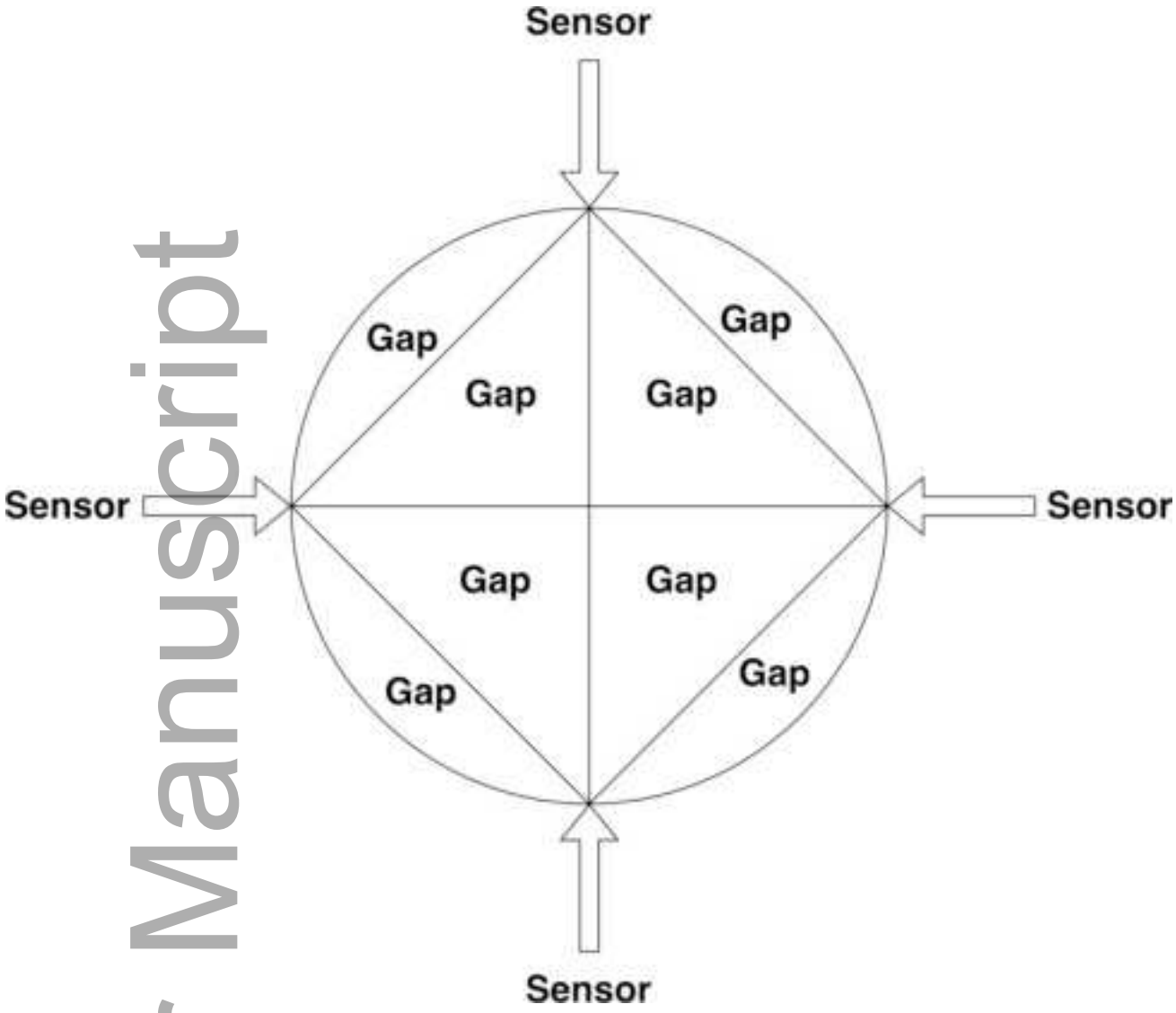

phor_12328_f2.png

phor_12328_f3.png

phor_12328_f4.png

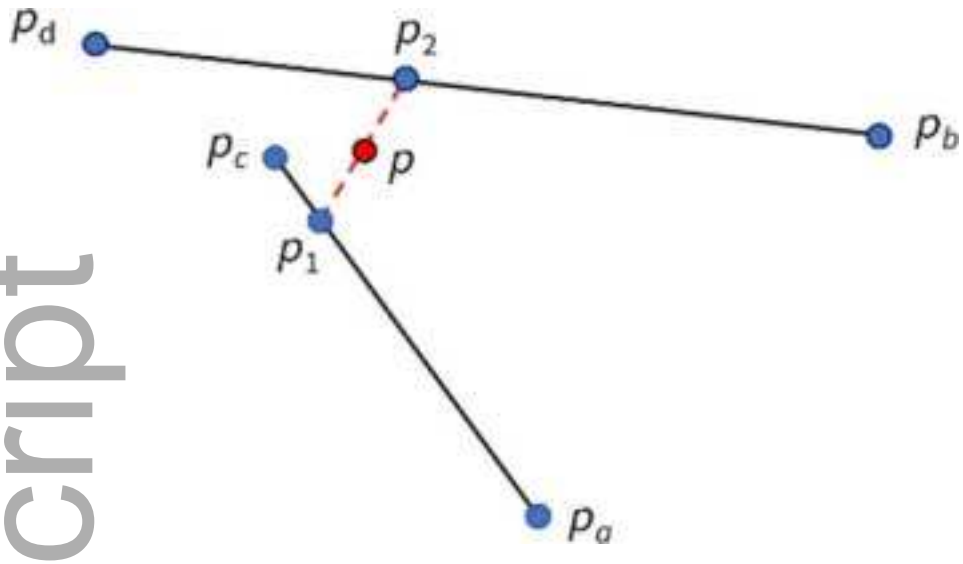

phor_12328_f5.png

phor_12328_f6a.png

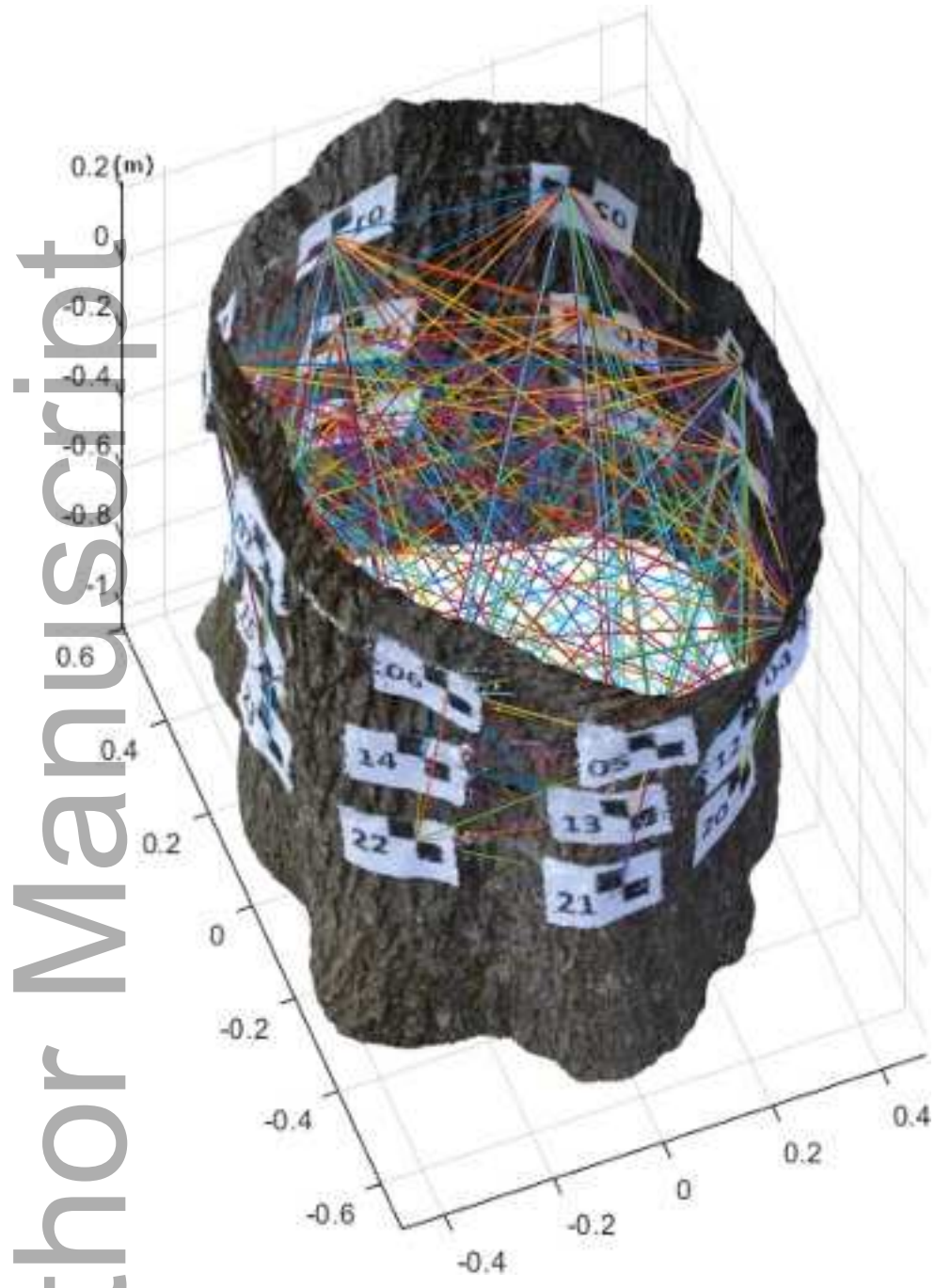

phor_12328_f6b.png

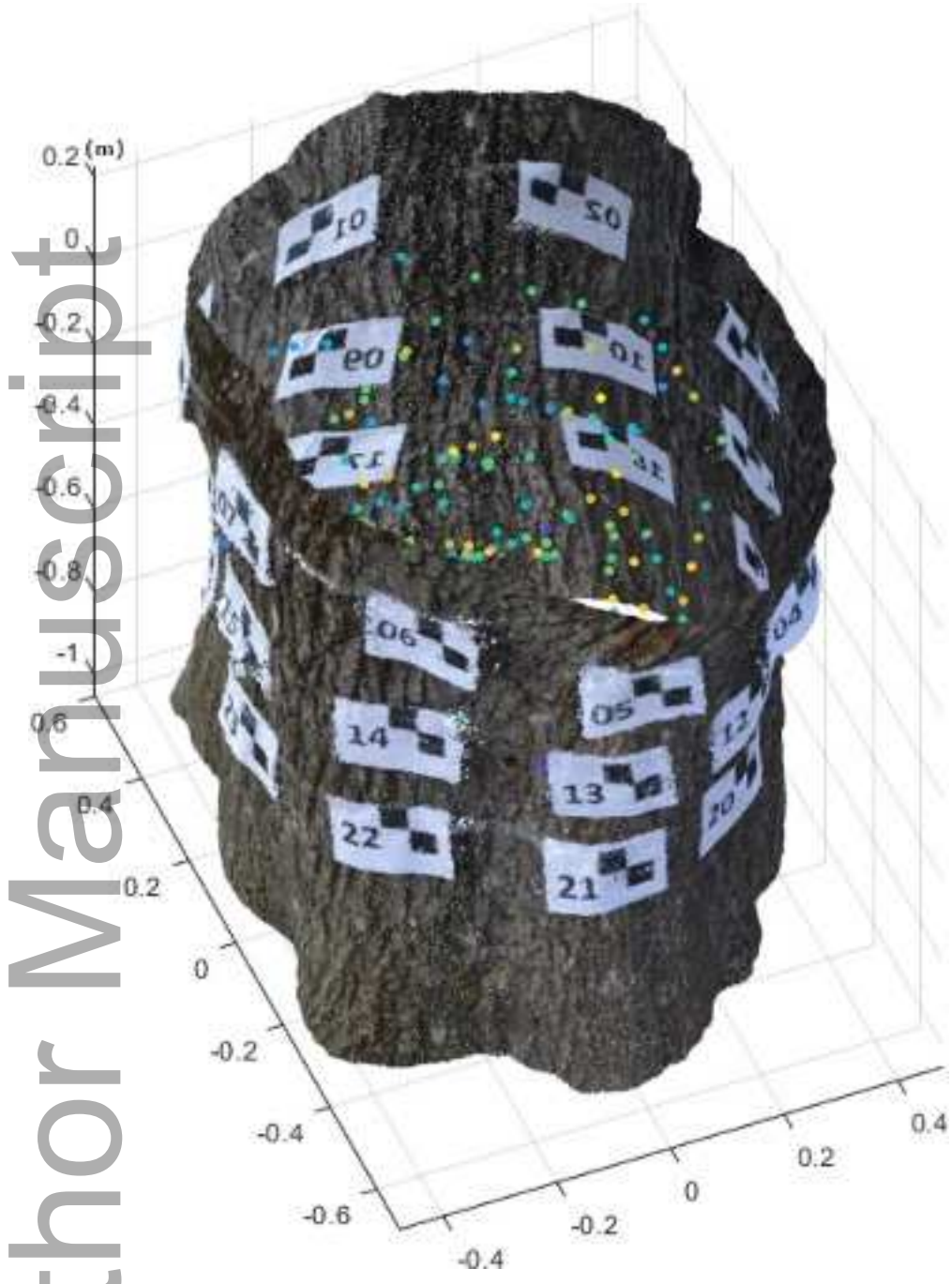

phor_12328_f6c.png

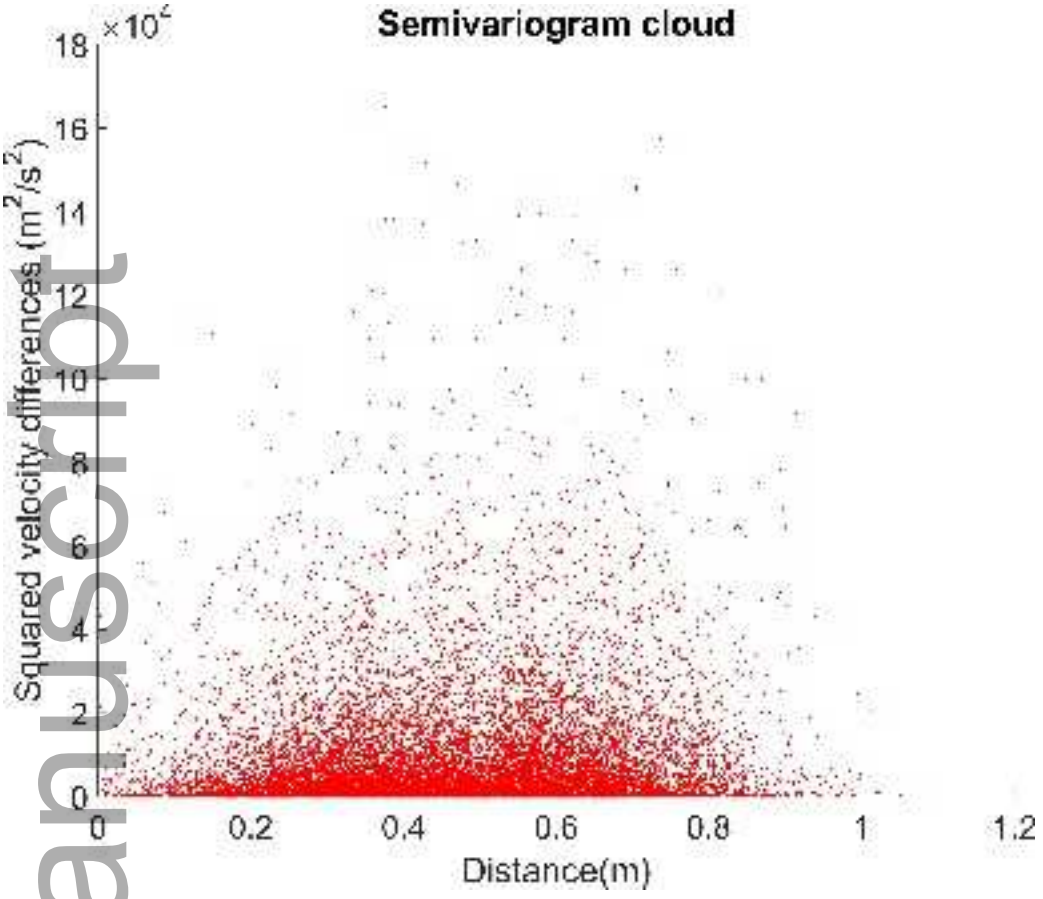

phor_12328_f7a.png

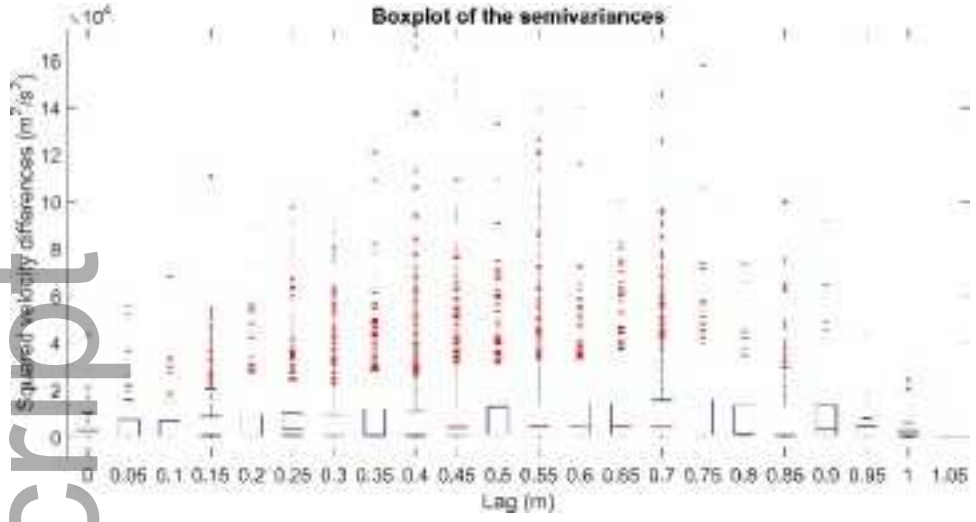

phor_12328_f7b.png

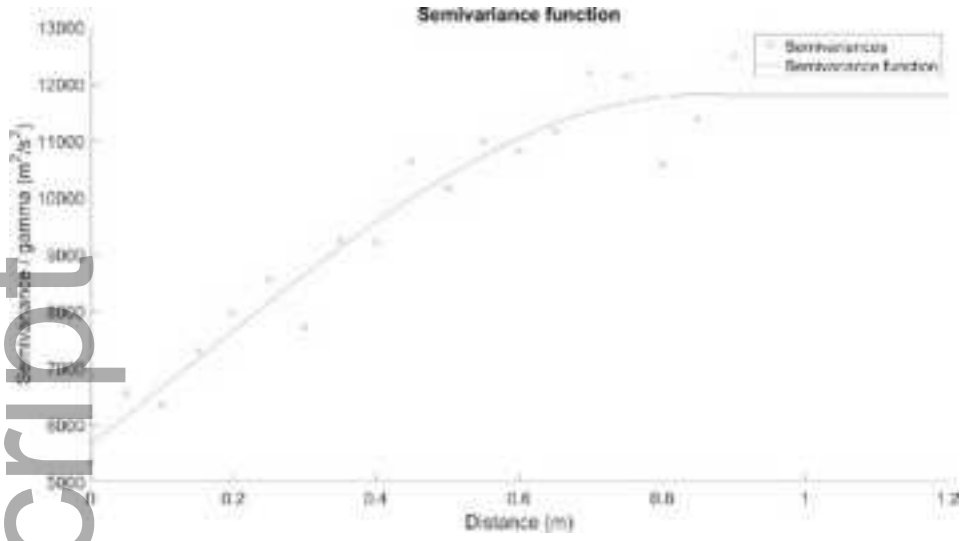

phor_12328_f7c.png

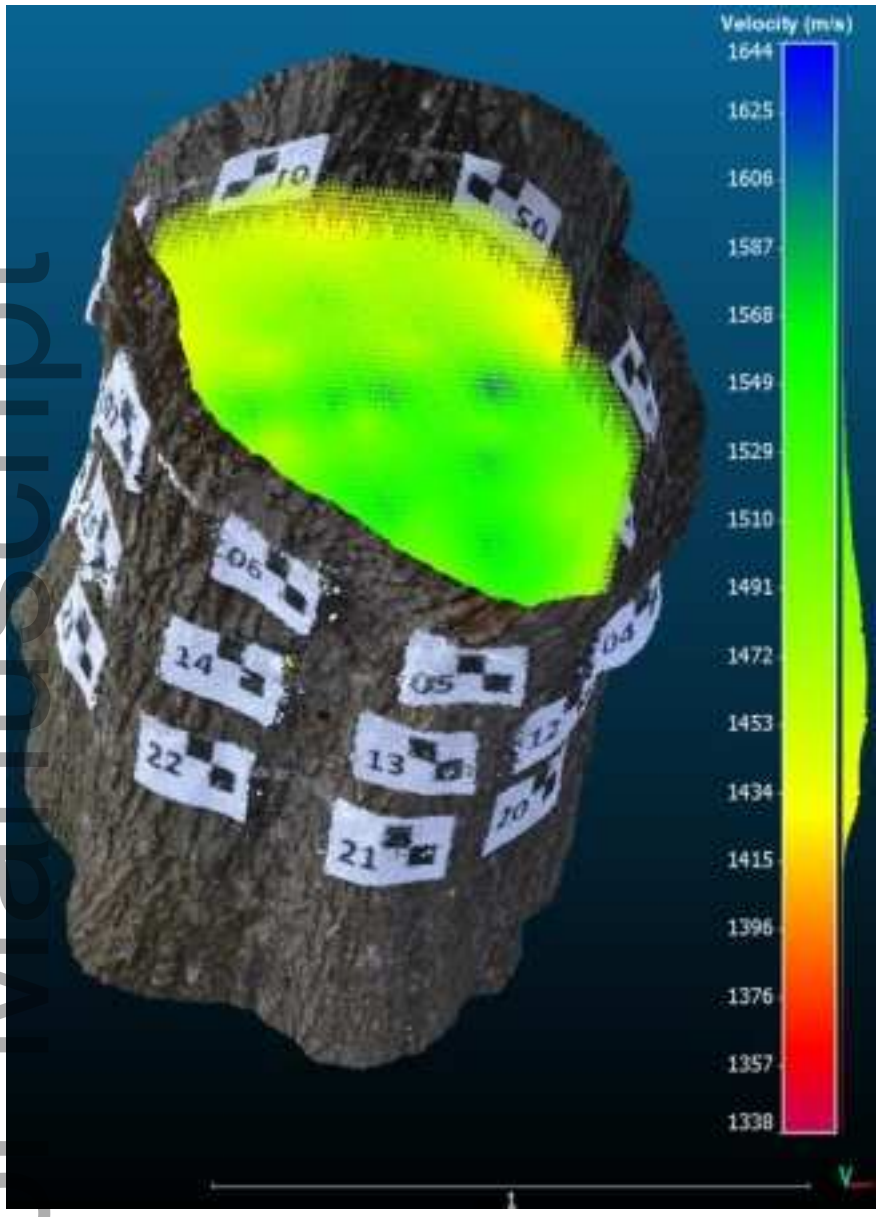

phor_12328_f8a.png

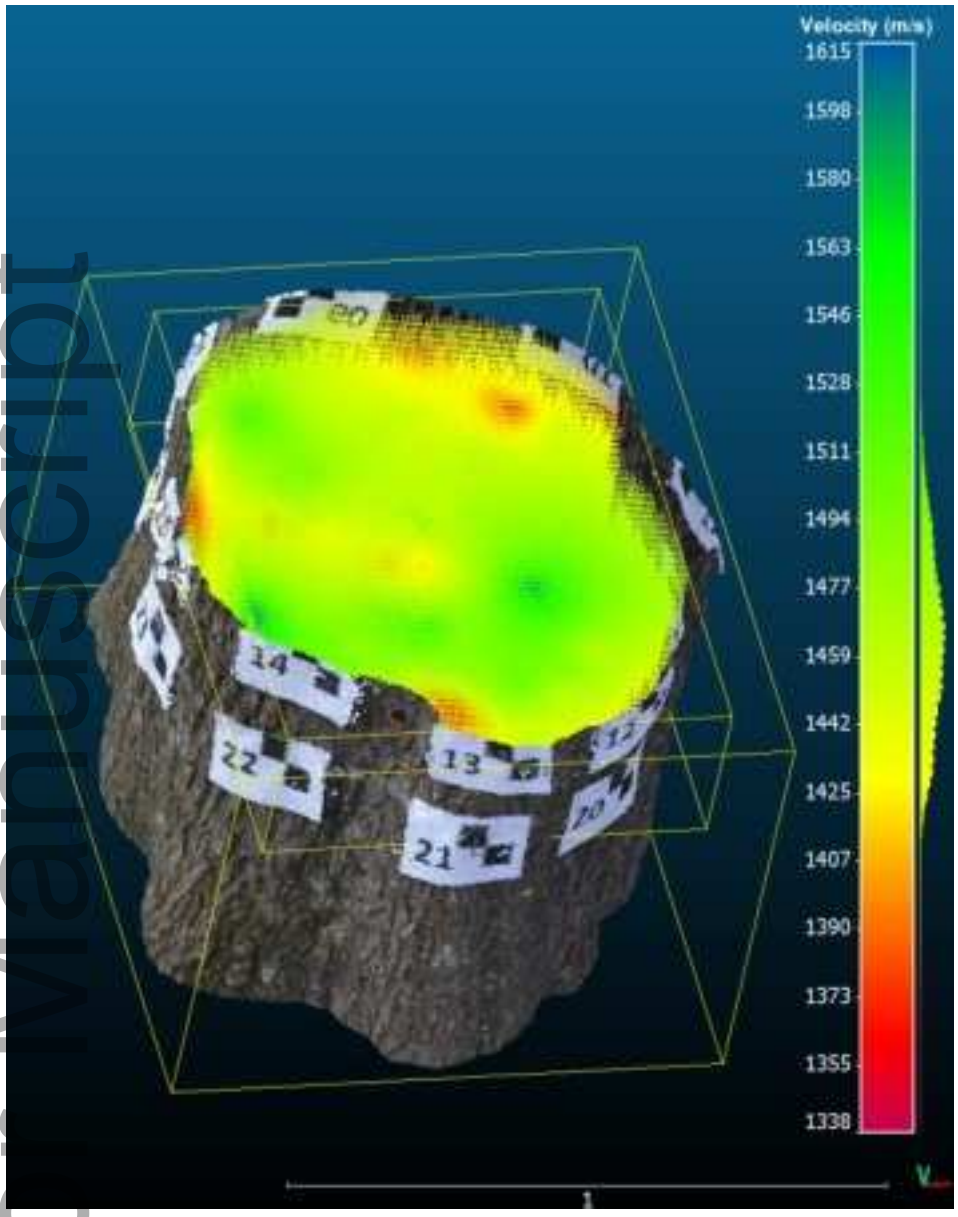

phor_12328_f8b.png

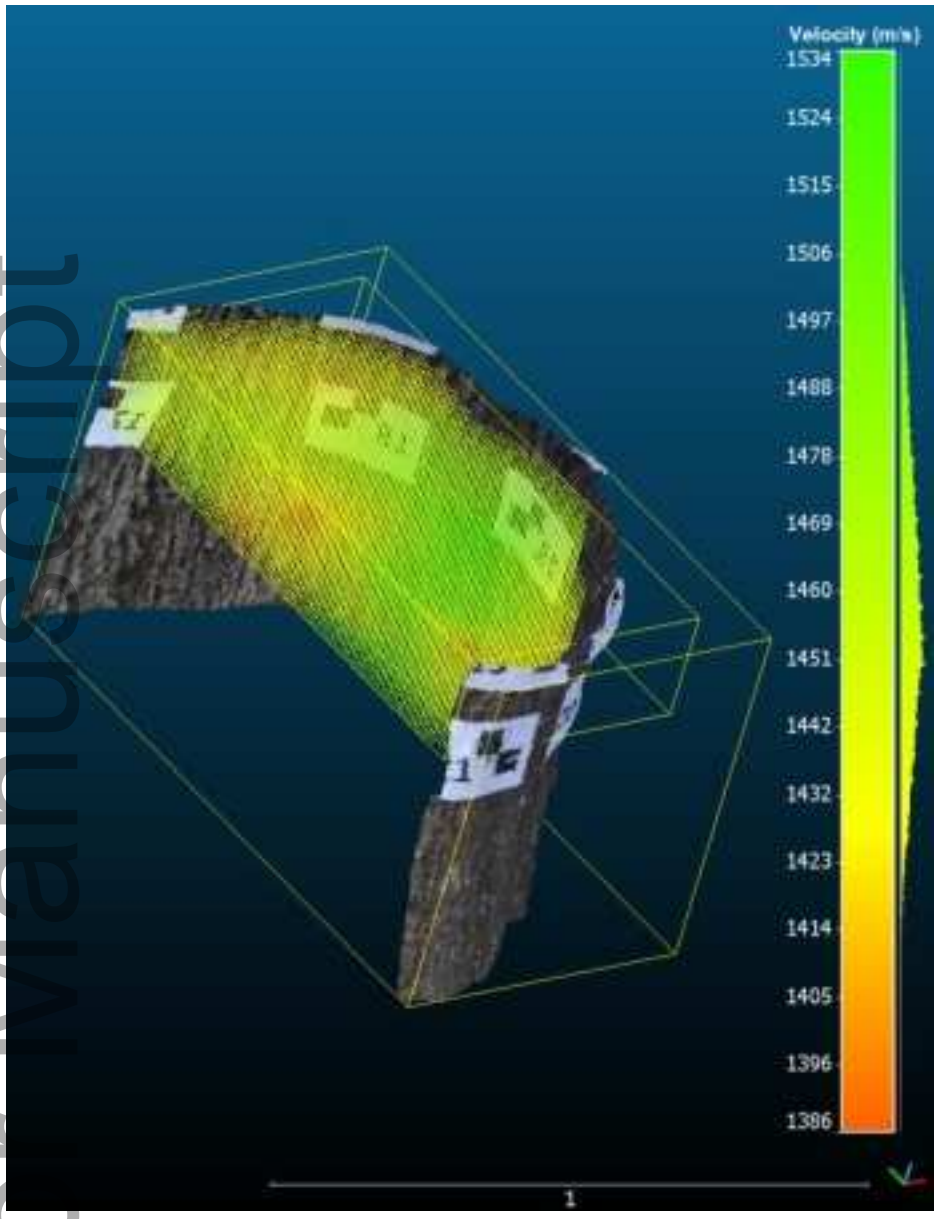

phor_12328_f8c.png

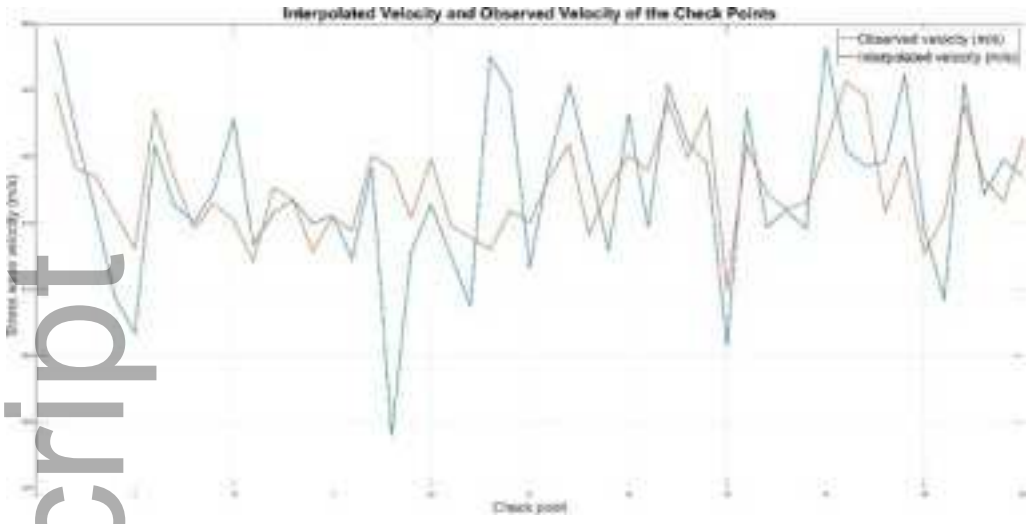

phor_12328_f9.png

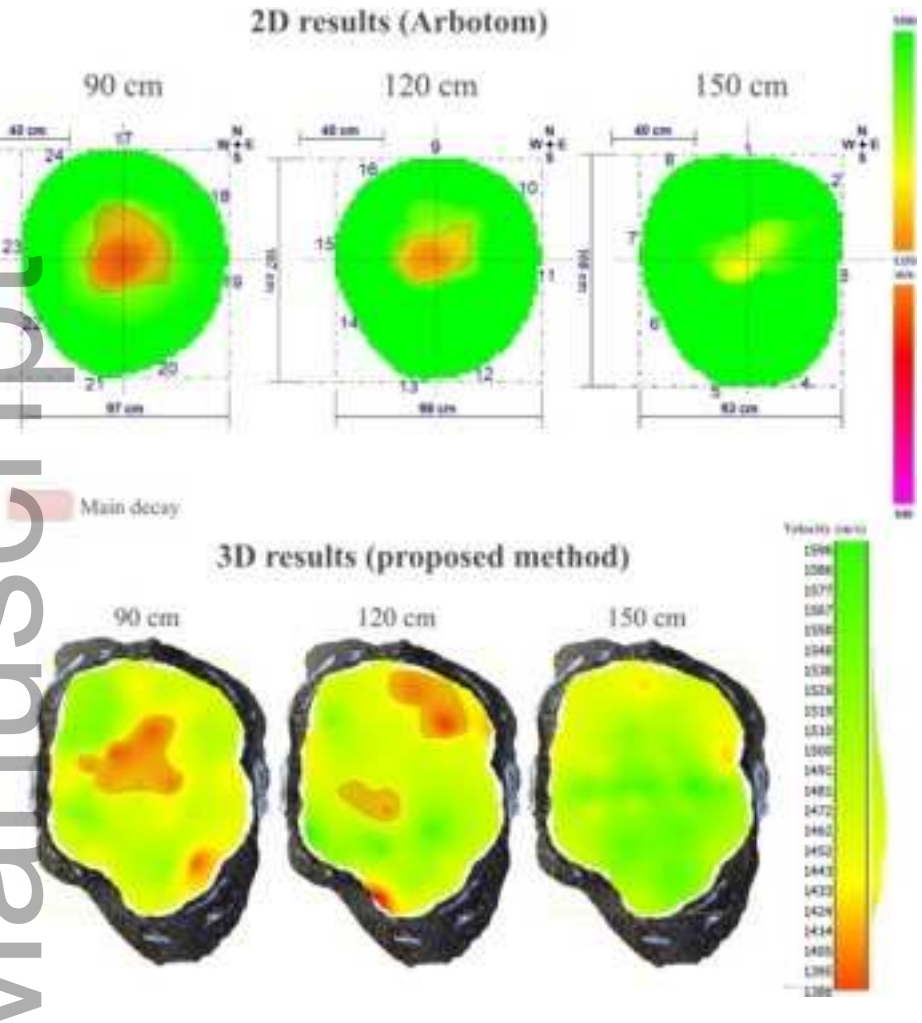

phor_12328_f10.png

Author/s:
Zhang, J;Khoshelham, K

Title:
3D RECONSTRUCTION OF INTERNAL WOOD DECAY USING PHOTOGRAMMETRY AND SONIC TOMOGRAPHY

Date:
2020-09

Citation:
Zhang, J. & Khoshelham, K. (2020). 3D RECONSTRUCTION OF INTERNAL WOOD DECAY USING PHOTOGRAMMETRY AND SONIC TOMOGRAPHY. PHOTOGRAMMETRIC RECORD, 35 (171), pp.357-374. https://doi.org/10.1111/phor.12328.